esa

ECOSPHERE

Monitoring pigment-driven vegetation changes in a low-Arctic tundra ecosystem using digital cameras

ALISON L. BEAMISH,[1,]† NICHOLAS C. COOPS,[2] TXOMIN HERMOSILLA,[2] SABINE CHABRILLAT,[3] AND BIRGIT HEIM[1]

[1]*Alfred Wegener Institute, Periglacial Research, Telegrafenberg A45, 14473 Potsdam, Germany*
[2]*Integrated Remote Sensing Studio (IRSS), Faculty of Forestry, University of British Columbia, 2424 Main Mall, Vancouver, British Columbia V6T1Z4 Canada*
[3]*Helmholtz Centre Potsdam (GFZ), German Research Centre for Geosciences, Telegrafenberg A17, 14473 Potsdam, Germany*

Citation: Beamish, A. L., N. C. Coops, T. Hermosilla, S. Chabrillat, and B. Heim. 2018. Monitoring pigment-driven vegetation changes in a low-Arctic tundra ecosystem using digital cameras. Ecosphere 9(2):e02123. 10.1002/ecs2.2123

Abstract. Arctic vegetation phenology is a sensitive indicator of a changing climate, and rapid assessment of vegetation status is necessary to more comprehensively understand the impacts on foliar condition and photosynthetic activity. Airborne and space-borne optical remote sensing has been successfully used to monitor vegetation phenology in Arctic ecosystems by exploiting the biophysical and biochemical changes associated with vegetation growth and senescence. However, persistent cloud cover and low sun angles in the region make the acquisition of high-quality temporal optical data within one growing season challenging. In the following study, we examine the capability of "near-field" remote sensing technologies, in this case digital, true-color cameras to produce surrogate in situ spectral data to characterize changes in vegetation driven by seasonal pigment dynamics. Simple linear regression was used to investigate relationships between common pigment-driven spectral indices calculated from field-based spectrometry and red, green, and blue (RGB) indices from corresponding digital photographs in three dominant vegetation communities across three major seasons at Toolik Lake, North Slope, Alaska. We chose the strongest and most consistent RGB index across all communities to represent each spectral index. Next, linear regressions were used to relate RGB indices and extracted leaf-level pigment content with a simple additive error propagation of the root mean square error. Results indicate that the green-based RGB indices had the strongest relationship with chlorophyll *a* and total chlorophyll, while a red-based RGB index showed moderate relationships with the chlorophyll to carotenoid ratio. The results suggest that vegetation color contributes strongly to the response of pigment-driven spectral indices and RGB data can act as a surrogate to track seasonal vegetation change associated with pigment development and degradation. Overall, we find that low-cost, easy-to-use digital cameras can monitor vegetation status and changes related to seasonal foliar condition and photosynthetic activity in three dominant, low-Arctic vegetation communities.

Key words: hyperspectral; low-Arctic; red, green, and blue indices; true-color digital photography; vegetation pigments.

Received 20 January 2018; accepted 24 January 2018. Corresponding Editor: Debra P. C. Peters.

† **E-mail:** abeamish@awi.de

INTRODUCTION

Changes to the functioning of Arctic ecosystems, such as shifts in photosynthetic activity, net primary productivity, and species composition influence global climate change and the resulting feedbacks (Zhang et al. 2007, Bhatt et al. 2010, Parmentier and Christensen 2013). Climatic changes have been accompanied by broad-scale shifts in Arctic vegetation community composition and species distribution, as well as fine-scale shifts in individual plant reproduction and

phenology (Walker et al. 2006, Bhatt et al. 2010, Elmendorf et al. 2012*a*, Bjorkman et al. 2015, Prevéy et al. 2017). Changes in vegetation phenology can impact overall ecosystem functioning as a result of mismatched species–climate interactions. This in turn can impact species photosynthetic activity and growth through increased vulnerability to events such as frost, soil saturation, or disruption to species chilling requirements (Inouye and McGuire 1991, Yu et al. 2010, Cook and Wolkovich 2012, Høye et al. 2013, Wheeler et al. 2015).

In Arctic ecosystems, snow pack conditions and timing of snowmelt, rather than temperature, are primary drivers of the onset of vegetation phenology (Billings and Bliss 1959, Bjorkman et al. 2015). Changing snowmelt dynamics due to changes in winter precipitation and spring temperatures have been shown to directly influence tundra vegetation phenology throughout the growing season (Bjorkman et al. 2015). Thus, the onset of the growing season, or the leaf-out stage, acts as a benchmark of phenology, and identification and characterization of this stage are key to understanding the overall and subsequent phenology and fitness of tundra vegetation (Iler et al. 2013, Wheeler et al. 2015). The timing of maximum expansion and elongation of leaves and stems and when vegetation is at, or near, peak photosynthetic activity, or peak greenness, are also important benchmarks of phenological phases. Peak greenness marks the climax of the growing season, the timing and magnitude of which can indicate ecosystem functioning, and acts as a benchmark for long-term monitoring of tundra productivity (Bhatt et al. 2010, 2013). A final benchmark of phenological phase is the end of the growing season, or senescence. In combination with leaf-out, senescence dictates growing season length and has implications for overall seasonal productivity and carbon assimilation (Park et al. 2016). Characterizing key biophysical properties of Arctic vegetation associated with these three benchmark phenological phases is important for accurate monitoring and quantification of local and regional changes in Arctic vegetation and in turn Arctic and global changes to energy and carbon cycling, as well as associated feedbacks. The presence and seasonal changes in vegetation pigment content can be used to infer biophysical properties including photosynthetic activity and foliar condition at key phenological phases of Arctic vegetation.

The major photosynthetic pigment groups of chlorophyll and carotenoids absorb strongly in the visible spectrum creating unique spectral signatures (Curran 1989, Gitelson and Merzlyak 1998, Gitelson et al. 2002, Coops et al. 2003). Chlorophyll pigments are the dominant factor controlling the amount of light absorbed by a plant and therefore photosynthetic potential, which ultimately dictates primary productivity. Carotenoids (carotenes and xanthophylls) are responsible for absorbing incident radiation and providing energy to the photosynthetic process and are often used to provide information on the physiological status of vegetation (Young and Britton 1990, Bartley and Scolnik 1995). The third major pigment group of anthocyanins (water-soluble flavonoids) has a less concise function in vegetation providing photoprotection (Steyn et al. 2002, Close and Beadle 2003), drought and freezing protection (Chalker-Scott 1999), and they have been shown to play a role in recovery from foliar damage (Gould et al. 2002). Photosynthetic pigments influence a wide range of plant functioning from photosynthetic efficiency to protective functions (Demmig-Adams and Adams 1996) and can be measured destructively through laboratory analysis or non-destructively using high spectral resolution remote sensing (Gitelson et al. 1996, 2001, 2002, 2006).

The development and degradation of chlorophyll pigments as a result of vegetation emergence, stress, or senescence causes a distinct shift in spectral signatures in the visible spectrum to shorter wavelengths due to a narrowing of the major chlorophyll absorption feature (550–750 nm) and an overall reduction in spectral absorption (Ustin and Curtiss 1990). Carotenoids (yellow to orange) and anthocyanins (blue to red) have less straightforward seasonal, and therefore spectral, shifts. The spectral absorption by carotenoid pigments can result in mixed or masked spectral absorption with chlorophyll signals due to overlapping absorption features in the visible spectrum (400–700 nm). Carotenoids and anthocyanins often have relatively higher concentrations in senesced and young leaves when chlorophyll concentrations are relatively low (Tieszen 1972, Sims and Gamon 2002, Stylinski et al. 2002). However, in general, the predictable

and distinct spectral features created by changes in vegetation pigment content allow inferences of ecological parameters such as photosynthetic activity, nutrient concentration, and biomass (Mutanga and Prins 2004, Mutanga and Skidmore 2004, Asner and Martin 2008, Ustin et al. 2009).

Of particular interest for in situ and laboratory spectroscopy of vegetation and phenology are the spectral characterization of the xanthophyll cycle (carotenoids) and the ratio between photosynthetic pigments of carotenoids and chlorophyll as they relate to radiation use efficiency and in turn radiative transfer models (Blackburn 2007, Garbulsky et al. 2011, Gamon et al. 2016). Radiative transfer models are used to simulate leaf and canopy spectral reflectance and transmittance, and have been the basis for the inverse determination of biophysical and biochemical parameters of vegetation based on spectral reflectance (Féret et al. 2011). Even at lower spectral resolution, the importance of pigments and pigment dynamics related to the xanthophyll cycle can be seen in available products for recent satellite missions; for example, the European Space Agency's (ESA) Sentinel-2 provides many pigment-driven vegetation indices (see https://www.sentinel-hub.com/develop/documentation/eo_products/Sentinel2EOproducts).

While highly valuable, in situ reflectance spectroscopy, like optical remote sensing, is challenging for remote Arctic field sites. Remote locations, challenges associated with field-based monitoring, and atmospheric and illumination conditions of optical satellite imagery of these areas limit available optical data, hindering phenological studies. To complement the use of airborne and satellite imagery to measure vegetation pigments and classify biophysical properties in Arctic ecosystems, the use of true-color digital photography and red, green, and blue (RGB) indices to infer photosynthetic activity and foliar condition is a promising area of study and should be examined (Anderson et al. 2016, Beamish et al. 2016). Research has shown that Arctic vegetation changes are complex with strong site and species-specific responses through space and time (Walker et al. 2006, Bhatt et al. 2010, Elmendorf et al. 2012*b*, Bjorkman et al. 2015, Prevéy et al. 2017). True-color digital photography represents both a simple and cost-effective way to increase data volume both spatially and temporally to capture site and species-specific responses. Data from consumer-grade digital cameras have extremely high spatial resolution and high data collection capabilities and are less weather dependent than airborne and optical satellite remote sensing as varying illumination can be easily corrected (Richardson et al. 2007, Nijland et al. 2014). Large-scale, true-color, repeatable digital photography networks in temperate ecosystems such as the PhenoCam network (http://phenocam.sr.unh.edu/webcam/) highlight the existing ecological applications of this method. Additional work by Richardson et al. (2007) and Coops et al. (2012) demonstrates the link between ground-based true-color camera systems and satellite-scale (Landsat and MODIS) observations. In addition to phenological parameters, well-established RGB indices derived from consumer-grade digital cameras have been shown to accurately identify vegetation cover in Arctic tundra and temperate forests (Richardson et al. 2007, Ide and Oguma 2010, Nijland et al. 2014, Beamish et al. 2016) and can be closely related to gross primary production in grasslands, temperate forests, Arctic tundra, and wetlands (Ahrends et al. 2009, Migliavacca et al. 2011, Westergaard-Nielsen et al. 2013, Anderson et al. 2016), as well as containing a sensitivity to changes in plant photosynthetic pigments (Ide and Oguma 2013).

In this study, we examine the capability of in situ, true-color digital photography to act as a surrogate for in situ spectral data in assessing pigment-driven vegetation changes associated with three key seasons representing early, peak, and late season, in three dominant, low-Arctic tundra vegetation communities. To do this, we asked the following research questions: (1) What are the relationships between RGB indices and in situ, pigment-driven spectral indices? (2) How do these relationships change with community type and season? (3) To what extent do the indices represent actual chlorophyll and carotenoid content? We conclude with proposing the RGB indices best suited as proxies for in situ spectral data for monitoring seasonal vegetation change and the related pigment dynamics in a low-Arctic tundra.

Methods

Study site

Data were collected at the Toolik Field Station (68°62.57′ N, 149°61.43′ W) on the North Slope of

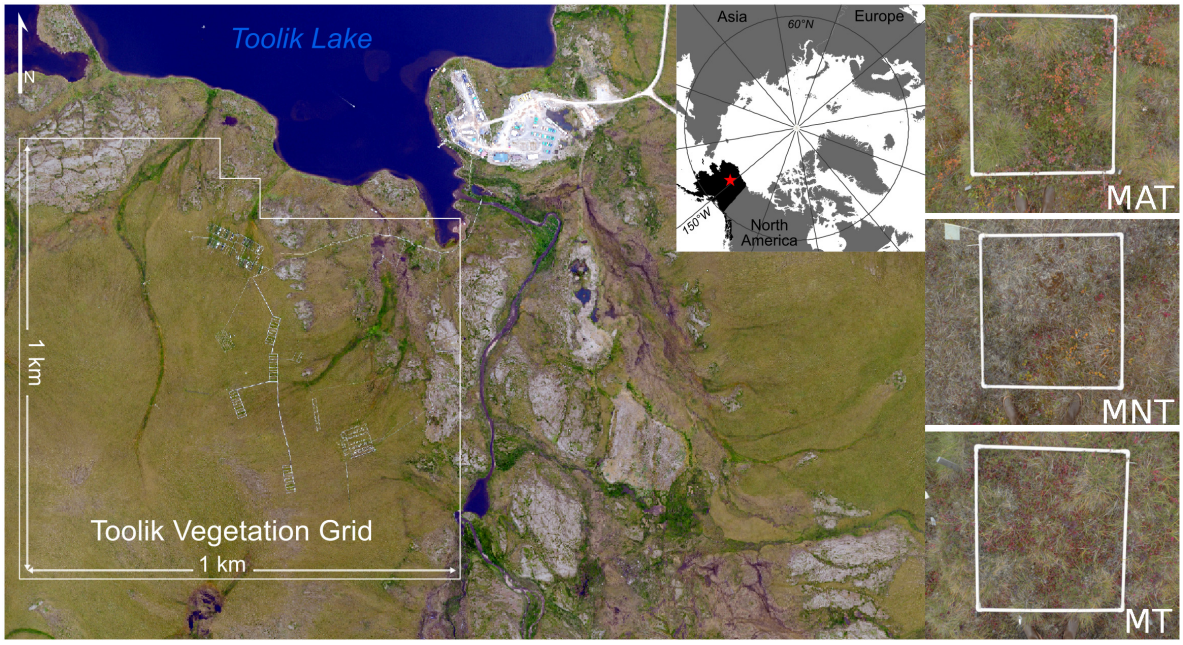

Fig. 1. Toolik Vegetation Grid located in the Toolik Research Area on the North Slope of the Brooks Range in northern Alaska and a late season example plots of the three vegetation communities monitored in the study. MAT, moist acidic tussock tundra; MNT, moist non-acidic tundra; MT, moss tundra.

the Brooks Range, in north central Alaska in the growing season of 2016. The Toolik Area is representative of the southern Arctic Foothills, a physiographic province of the North Slope (Walker et al. 1989). Vegetation is a combination of moist tussock tundra, wet sedge meadows, and dry upland heaths. Data were acquired in the Toolik Vegetation Grid, a 1 × 1 km long-term monitoring site established by the National Science Foundation (NSF) as part of the Department of Energy's R4D (Response, Resistance, Resilience, and Recovery to Disturbance in Arctic Ecosystems) project (Fig. 1). Vegetation monitoring plots (1 × 1 m) are positioned in close proximity to equally spaced site markers delineating the intersection of the Universal Transverse Mercator (UTM) coordinates and each point within the grid. A subset of the grid was sampled for the purpose of this study representing three distinct and dominant vegetation communities as defined by Bratsch et al. (2016) (Fig. 1). The communities include moist acidic tundra (MAT), moist non-acidic tundra (MNT), and moss tundra (MT). A detailed description and representativeness (% cover of the Toolik Vegetation Grid) of the three vegetation communities sampled within the Long-term Toolik Vegetation Grid are shown in Table 1.

Digital photographs

In order to capture the three major seasons of early, peak, and late, we acquired true-color digital photographs on three days in the 2016 growing season (June 16, day of year [DOY] 165; July 11, DOY 192; August 17, DOY 229). Images were taken at nadir approximately 1 m off the ground with a white 1 × 1 m frame for registration of off nadir images (Fig. 1). According to the Toolik Lake Environmental Data Centre (https://toolik.alaska.edu/edc/, 2017) phenology record that monitors 15 dominant species at the Toolik Field Station, the first image acquisition date occurred two weeks after the average date of first leaf-out (May 29, DOY 149) accurately capturing the peak of the early leaf-out phase. The second acquisition took place one week after average date of last flower petal drop (July 3, DOY 185) and within one week of recorded full green-up (end of June). The final acquisition took place three weeks after average first day of fall color change (July 27, DOY 209) and within the range of recorded peak fall colors (mid-August).

Table 1. Description of the three vegetation communities monitored in this study.

Community	Description	Detailed description	% cover
Moist acidic tussock tundra	Occurs on soils with pH < 5.0–5.5 and is dominated by dwarf erect shrubs such as *Betula nana* and *Salix pulchra*, graminoids species (*Eriophorum vaginatum*), and acidophilous mosses	*Betula nana–Eriophorum vaginatum*. Dwarf-shrub, sedge, moss tundra (shrubby tussock tundra dominated by dwarf birch, *Betula nana*). Mesic to subhygric, acidic, moderate snow. Lower slopes and water-track margins. Mostly on Itkillik I glacial surfaces *Salix pulchra–Carex bigelowii*. Dwarf-shrub, sedge, moss tundra (shrubby tussock tundra dominated by diamond-leaf willow, *Salix pulchra*). Subhygric, moderate snow, lower slopes with solifluction	6.1
Moist non-acidic tundra	Dominated by mosses, graminoids (*Carex bigelowii*), and prostrate dwarf shrubs (*Dryas integrifolia*)	*Carex bigelowii–Dryas integrifolia*, typical subtype; *Tomentypnum nitens–Carex bigelowii*, *Salix glauca* subtype: nontussock sedge, dwarf-shrub, moss tundra (moist non-acidic tundra). Mesic to subhygric, non-acidic (pH > 5.5), shallow to moderate snow. Solifluction areas and somewhat unstable slopes. Some south-facing slopes have scattered glaucous willow (*Salix glauca*)	5.8
Mossy tussock tundra	A moist acidic tussock tundra-type community dominated by sedges (*E. vaginatum*) and abundant *Sphagnum* spp.	*Eriophorum vaginatum–Sphagnum; Carex bigelowii–Sphagnum:* tussock sedge, dwarf-shrub, moss tundra (tussock tundra, moist acidic tundra). Mesic to subhygric, acidic, shallow to moderate snow, stable. This unit is the zonal vegetation on fine-grained substrates with ice-rich permafrost. Some areas on steeper slopes with solifluction are dominated by Bigelow sedge (*Carex bigelowii*)	54.2

Images were acquired with a consumer-grade digital camera (Panasonic DM3 LMX, Osaka, Japan) in raw format, between 10:00 h and 14:00 h, under uniform cloud cover to reduce the influence of shadow and illumination differences. The digital camera collects color values by means of the Bayer matrix (Bayer 1976) with individual pixels coded with a red, green, and blue value between 0 and 256. RGB values of each pixel in each image were extracted using ENVI+IDL (Version 4.8; Harris Geospatial, Boulder, Colorado, USA). To reduce the impact of non-nadir acquisitions, photo registration was undertaken using the 1 × 1 m apart. Table 2 shows the normalized RGB channels and RGB indices calculated based on the normalized red, green, and blue values of the digital photographs, hereafter referred to as RGB indices.

Table 2. Calculated red, green, and blue (RGB) indices from RGB channels of digital photographs.

Index	Formula	Source
nG	G/(R+B+G)	
nR	R/(R+B+G)	
nB	B/(R+B+G)	
GR	nG/nR	
GB	nG/nB	
2G-RB	2 × nG − (nR + nB)	Richardson et al. (2007)

Digital camera indices 2G-RB and nG have been used to monitor vegetation phenology and biomass extensively (Richardson et al. 2007, Ide and Oguma 2013, Beamish et al. 2016). Additionally, we defined new RGB indices to examine their representativeness to selected pigment-driven spectral indices (Table 3). We chose these RGB indices as they represented as closely as possible the mathematical formulas of selected pigment-driven indices presented in the *Field-based spectral data* section.

Field-based spectral data

Within one week of the digital photographs, field-based spectral measurements of each vegetation plot were acquired using a GER 1500 field spectroradiometer (Spectra Vista Corporation, New York, New York, USA). Spectral data were

Table 3. Pseudo pigment-driven red, green, and blue (RGB) indices calculated from RGB channels of digital photographs.

Indices	Formula
nBG	(nB−nG)/(nB+nG)
nRG	(nR−nG)/(nR+nG)
RGr	((nR−nG)/nR)
nG^{-1}	(1/nG)
2R-GB	2 × nR − (nG + nB)

acquired on June 14 (DOY 165), July 8 (DOY 189), and August 23 (DOY 235) in 2016 with a spectral range of 350–1050 nm, 512 bands, a spectral resolution of 3 nm, a spectral sampling of 1.5 nm, and an 8° field of view. Data were acquired under clear weather conditions between 10:00 and 14:00 local time corresponding to the highest solar zenith angle. In each plot, radiance data were acquired at nadir approximately 1 m off the ground resulting in an approximately 15 cm diameter ground instantaneous field of view. To reduce noise and characterize the spectral variability in each plot, an average of nine point measurements of upwelling radiance (L_{up}) in each of the 1 × 1 m plots was used. Downwelling radiance (L_{down}) was measured as the reflection from a white Spectralon© plate. Surface reflectance (R) was processed as:

$$R = \frac{L_{up}}{L_{down}} \times 100 \quad (1)$$

Reflectance spectra (0–100%) were preprocessed with a Savitzky-Golay smoothing filter (n = 11), and to remove sensor noise at the spectral limits of the radiometer, data were subset to 400–985 nm.

Using the spectral reflectance data, we calculated common pigment-driven vegetation indices, focusing on vegetation color, and those produced as remote sensing products by the ESA and the North American Space Agency (NASA); a brief description of each is provided below (Table 4). The indices that were calculated from the field-based GER data are hereafter referred to as pigment-driven spectral indices.

The Photochemical Reflectance Index (PRI) is an indicator of photosynthetic radiation use efficiency and was first proposed by Gamon et al. (1992). The Plant Senescence Reflectance Index (PSRI) is sensitive to senescence-induced reflectance changes from changes in chlorophyll and carotenoid content and was proposed by Merzlyak et al. (1999). The Pigment Specific Simple Ratios (PSSRa and b) aim to model chlorophyll *a* and *b*, respectively (Blackburn 1998, 1999, Sims and Gamon 2002). Chlorophyll Carotenoid Index (CCI) was developed to track the phenology of photosynthetic activity of evergreen species by Gamon et al. (2016). The carotenoid reflectance indices (CRI1 and CRI2) use the reciprocal reflectance at 508 and 548 nm and 508 and 698 nm, respectively, in order to remove the effect of chlorophyll (Gitelson et al. 2002). The anthocyanin reflectance indices (ARI1 and ARI2) developed by Gitelson et al. (2001, 2006) are designed to reduce the influence of chlorophyll absorption to isolate the anthocyanin absorption by taking the difference between the reciprocal of green (550 nm) and the red-edge (700 nm). ARI2 includes a multiplication by the near infrared (NIR) to reduce the influence of leaf thickness and density.

Vegetation pigment concentration

To estimate how accurately plot-level indices represent actual leaf-level pigment content, leaves and stems (n = 213) of the dominant vascular species in a subset of the sampled plots were collected at early, peak, and late season for chlorophyll and carotenoid analysis. Samples were placed in porous tea bags and preserved in a silica gel desiccant in an opaque container for up to 3 months until pigment extraction (Esteban et al. 2009). Each sample was homogenized by grinding with a mortar and pestle. Approximately 1.00 mg (±0.05 mg) of homogenized sample was placed into a vial with 2 mL of

Table 4. Pigment-driven spectral indices.

Indices	Short	Formula	Source
Photochemical Reflectance Index	PRI	$(\rho_{533} - \rho_{569})/(\rho_{533} + \rho_{569})$	Gamon et al. (1992)
Plant Senescence Reflectance Index	PSRI	$(\rho_{678} - \rho_{498})/\rho_{748}$	Merzlyak et al. (1999)
Pigment Specific Simple Ratio	PSSR	PSSRa = ρ_{800}/ρ_{671} PSSRb = ρ_{800}/ρ_{652}	Blackburn (1998, 1999); Sims and Gamon (2002)
Chlorophyll Carotenoid Index	CCI	$(\rho_{531} - \rho_{645})/(\rho_{531} + \rho_{645})$	Gamon et al. (2016)
Carotenoid Reflectance Index 1	CRI1	$(1/\rho_{508}) - (1/\rho_{548})$	Gitelson et al. (2002)
Carotenoid Reflectance Index 2	CRI2	$(1/\rho_{508}) - (1/\rho_{698})$	Gitelson et al. (2002)
Anthocyanin Reflectance Index 1	ARI1	$(1/\rho_{550}) - (1/\rho_{700})$	Gitelson et al. (2001)
Anthocyanin Reflectance Index 2	ARI2	$\rho_{800} \times [(1/\rho_{550}) - (1/\rho_{700})]$	Gitelson et al. (2001)

dimethylformamide (DMF). Vials were then wrapped in aluminum foil to eliminate any degradation of pigments due to UV light and stored in a fridge (4°C) for 24 h. Samples were measured into a cuvette prior to spectrophotometric analysis. Bulk pigment concentrations were then estimated using a spectrophotometer measuring absorption at 646.8, 663.8, and 480 nm (Porra et al. 1989). Absorbance (A) values at specific wavelengths were transformed into μg/mg concentrations of chlorophyll *a*, Chl_a; chlorophyll *b*, Chl_b; total chlorophyll, Chl_{a+b}; carotenoids, Car, using the following equations:

$$\text{Chl}_a = 12.00 \times A^{663.8} - 3.11 \times A^{646.8} \quad (2)$$

$$\text{Chl}_b = 20.78 \times A^{646.8} - 4.88 \times A^{663.8} \quad (3)$$

$$\text{Chl}_{a+b} = 17.67 \times A^{646.8} + 7.12 \times A^{663.8} \quad (4)$$

$$\text{Car} = \left(A^{480} - \text{Chl}_a\right)/245 \quad (5)$$

The chlorophyll *a* to chlorophyll *b* ($\text{Chl}_{a:b}$) and the chlorophyll to carotenoid ratios (Chl:Car) were calculated by dividing Eq. 2 by Eq. 3 and Eq. 4 by Eq. 5, respectively. Pigment concentration was calculated as the average concentration of the dominant species in each plot.

Data analysis

We examined the potential of digital camera RGB data as a proxy for identified pigment-driven vegetation indices using existing and new RGB indices. Simple linear regression was performed between RGB indices defined in Tables 2 and 3, and hyperspectral PRI, PSRI, PSSR, CCI, CRI, and ARI indices defined in Table 4 (Appendix S1: Table S1). The RGB and spectral indices from significant RGB/spectral linear regressions were then chosen for linear regression with Chl_a, Chl_b, $\text{Chl}_{a:b}$, and Car:Chl for each vegetation community to explore how well the chosen indices represent actual leaf-level pigment content.

As we assume RGB indices can be used in place of pigment-driven spectral indices, we wanted to include the error associated with spectral indices as a proxy for leaf-level pigments to more accurately estimate uncertainties. To do this, we used a simple additive error propagation of root mean square error of the selected RGB/pigment and spectral/pigment regressions using the following equations:

$$\text{RMSE} = \sqrt{\frac{\sum_{t=1}^{n}\left(X_{\text{obs},t} - X_{\text{model},t}\right)^2}{n}} \quad (6)$$

$$\text{RMSE}_{\text{prop}} = \sqrt{\left(\text{RMSE}_{z\sim y}\right)^2 + \left(\text{RMSE}_{x\sim y}\right)^2} \quad (7)$$

where RMSE is the root mean square error, $X_{\text{obs},t}$ and $X_{\text{model},t}$ are the actual and predicted values of the linear regression *t*, respectively, and where $\text{RMSE}_{\text{prop}}$ is the propagated RMSE of RGB~pigment regressions using the RMSE of the RGB~pigment regressions ($\text{RMSE}_{z\sim y}$) and the RMSE of the spectral~pigment regressions ($\text{RMSE}_{x\sim y}$; Appendix S1: Table S2). All analyses were performed in R (R Development Core Team 2007), and an alpha of 0.05 was used.

Results

RGB indices as a surrogate for pigment-driven spectral indices

The strength of the relationships between the RGB indices and the pigment-driven spectral indices was variable between vegetation communities (Appendix S1). The most consistent and strongest regressions across the three vegetation communities were selected and are presented in Table 5 and Fig. 2. The strongest three regressions were observed between RGr and ARI2 in MT ($R^2 = 0.77$, $P < 0.01$, RMSE = 0.04), followed by RG and PSRI in MAT ($R^2 = 0.75$, $P < 0.01$, RMSE = 0.05) and MNT ($R^2 = 0.75$, $P < 0.01$, RMSE = 0.04; Fig. 2). PSRI had the strongest relationships across the three communities, while the carotenoid reflectance indices of CRI1 and CRI2 and the anthocyanin index of ARI1 had the weakest relationships. In general, MT had the strongest and most consistent regressions across all indices followed by MAT and finally MNT. We chose the following six RGB indices, 2G-RB, 2R-GB, nG, nG^{-1}, RG, and RGr, representing the pigment-driven indices of PSSRb, PRI, PSSRa, CCI, PSRI, and ARI2, respectively, for linear regression with leaf-level pigment content.

RGB indices as a surrogate for leaf-level pigment content

The relationships between selected RGB indices and pigment content suggest high variability in both fit and uncertainty across the three vegetation communities (Table 6). In general, the indices

Table 5. The most consistent, significant linear regressions between red, green, and blue (RGB) indices and pigment-driven spectral indices in the three communities.

		MAT			MNT			MT		
Spectral	RGB	R^2	*P*-value	RMSE	R^2	*P*-value	RMSE	R^2	*P*-value	RMSE
PRI	2R-GB	**0.46**	**<0.01**	**0.04**	0.29	<0.01	0.04	**0.53**	**<0.01**	**0.03**
PSRI	RG	**0.78**	**<0.01**	**0.05**	**0.75**	**<0.01**	**0.04**	**0.70**	**<0.01**	**0.05**
PSSRa	nG	**0.72**	**<0.01**	**0.01**	**0.60**	**<0.01**	**0.01**	**0.71**	**<0.01**	**0.01**
PSSRb	2G-RB	**0.64**	**<0.01**	**0.04**	**0.53**	**<0.01**	**0.03**	**0.51**	**<0.01**	**0.03**
CCI	nG^{-1}	**0.56**	**<0.01**	**0.04**	**0.58**	**<0.01**	**0.02**	**0.73**	**<0.01**	**0.02**
CRI1	GB	**0.40**	**<0.01**	**0.18**	0.16	**0.02**	0.14	0.34	<0.01	0.14
CRI2	RB	0.09	<0.01	0.05	−0.01	0.43	0.04	0.17	0.03	0.02
ARI1	RG	0.30	**<0.01**	0.10	0.17	**0.01**	0.07	**0.42**	**<0.01**	**0.07**
ARI2	RGr	**0.63**	**<0.01**	**0.06**	**0.43**	**<0.01**	**0.04**	**0.77**	**<0.01**	**0.04**

Note: Bold values represent moderate or stronger ($R^2 > 0.40$) significant linear regressions.

performed best across all communities when predicting Chl_a with the strongest observed in MNT. nG, representing PSSRa, had the single strongest regression with Chl_a in MNT ($R^2 = 0.61$, $P < 0.01$, RMSE-P = 0.89), and this relationship was also moderate in MAT and MT. Chl_{a+b} and $Chl_{a:b}$ also showed weak to moderate correlations, but performance across communities was more variable than Chl_a. Both Chl_{a+b} and $Chl_{a:b}$ showed moderate correlations with all indices except 2R-GB in MNT and MAT, respectively. 2R-GB, representing PRI, also had a moderate relationship with Chl: Car in MT ($R^2 = 0.53$, $P < 0.01$, RMSE = 0.21) but poor performance in the other two communities. The indices performed worst when predicting Chl_b with $R^2 \leq 0.27$ in all cases.

Discussion

The relationships between selected RGB indices and pigment-driven spectral indices support the capability of digital cameras to act as a surrogate for in situ spectral data and for the study of seasonal vegetation changes associated with pigment dynamics in dominant low-Arctic vegetation communities. Evidence for the capability of digital cameras as an ecological monitoring tool of vegetation phenology, biomass, and productivity and the relationships of these parameters to spectrally derived vegetation indices exists in a variety of ecosystems (Ahrends et al. 2009, Coops et al. 2010, Ide and Oguma 2010, Migliavacca et al. 2011, Westergaard-Nielsen et al. 2013, Nijland et al. 2014, Anderson et al. 2016, Beamish et al. 2016). Our study adds to this knowledge base by expanding to pigment-driven vegetation indices chosen for their indication of photosynthetic efficiency, a parameter of high interest in vegetation remote sensing. In addition, we showcase the utility of a ground-based camera system in an ecosystem characterized by challenging acquisition conditions for spectral data.

There are some technical considerations when using these types of digital cameras that need to be considered such as consumer-grade digital cameras typically have limited range charge couple device/complementary metal oxide semiconductor sensors and employ automatic exposure adjustments with changing environmental brightness and local illumination. This in turn affects the comparability of images collected under different conditions; however, this can be overcome through the use of band ratios which are insensitive to brightness. Local illumination differences caused by direct sunlight can still introduce error; however, the Arctic is subject to unique illumination conditions because of the low solar zenith angle, long periods of daylight, and frequent cloud cover leading to frequent diffuse illumination conditions. Previous research has suggested collection of data under uniform cloud cover (diffuse conditions) is ideal (Ide and Oguma 2010). All images in this study were collected under uniform cloud cover by choice; however, when considering a framework of high-frequency (daily or hourly) data collection, these phenomena should be taken into consideration. Additionally, this study does not take into account the impact of atmospheric scattering common in shorter wavelengths (blue) of air- and space-borne platforms. This phenomenon

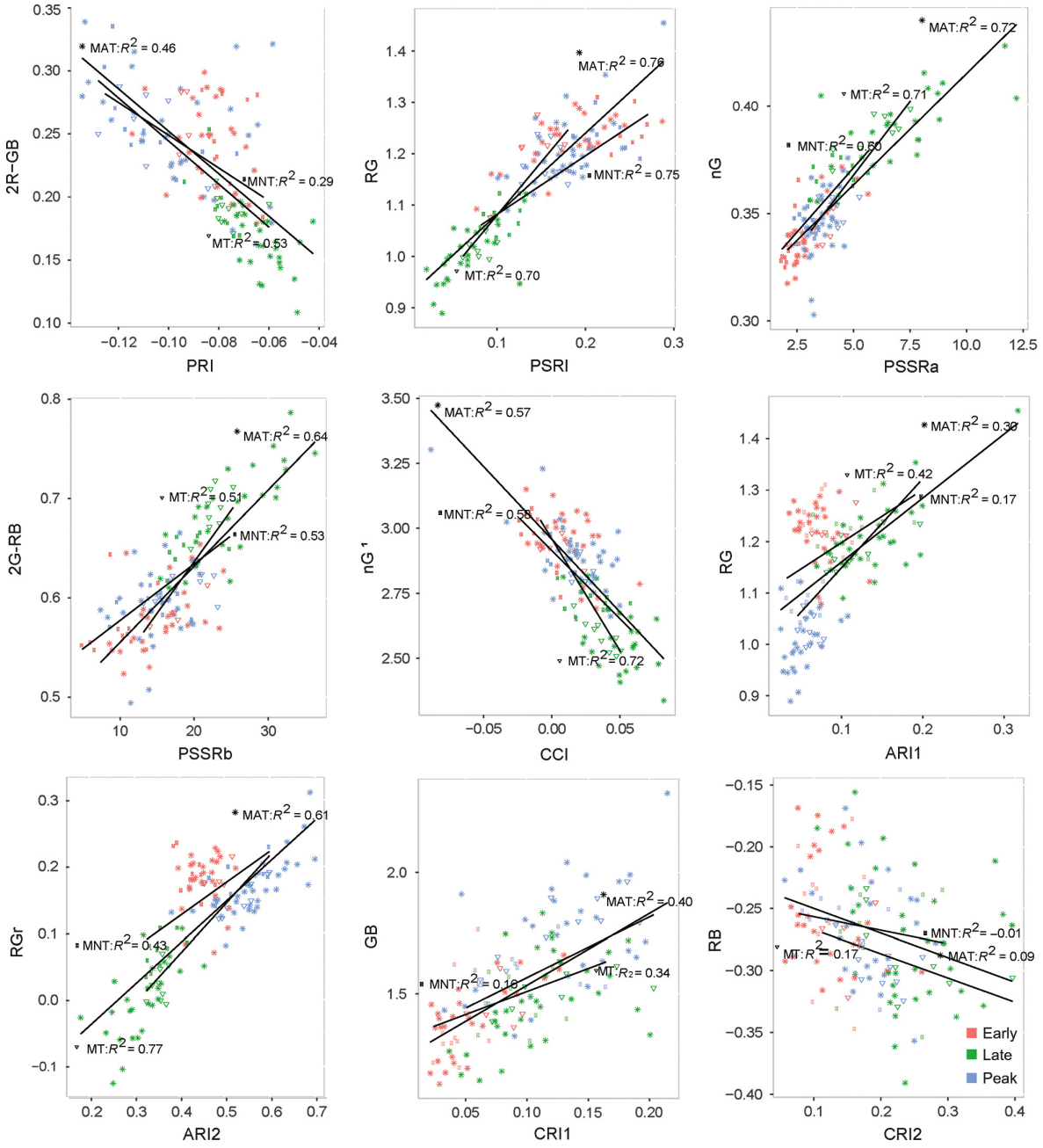

Fig. 2. Simple linear regression between the six best RGB indices and pigment-driven spectral indices across three seasons in each community type. MAT, moist acidic tussock tundra; MNT, moist non-acidic tundra; MT, moss tundra; RMSE, root mean square error.

would presumably reduce the correlation in the blue channel, and thus, its use should be minimized when inferring relationships between air- and space-borne platforms. However, the use of the blue channel in ground-based remote sensing as in this study is less of a concern as atmospheric scattering is minimal at this near-sensing scale. Another consideration is that, digital cameras contain what is known as a Bayer color filter array that combines one blue, one red, and two

Table 6. Simple linear regression between the selected red, green, and blue (RGB) indices and the spectral index they are representing in parentheses, and pigment content with the propagated mean absolute percentage error (MAPE-P).

Pigment µg/mg	Veg	RGB (spectral)											
		2G-RB (PSSRb)				2R-GB (PRI)				nG (PSSRa)			
(a)		R^2	*P*-value	RMSE	RMSE-P	R^2	*P*-value	RMSE	RMSE-P	R^2	*P*-value	RMSE	RMSE-P
Chl_a	MAT	0.38	0.00	0.31	0.48	0.17	0.02	0.35	0.52	0.39	0.00	0.30	0.42
	MNT	**0.59**	**0.01**	**0.12**	**0.22**	0.06	0.26	0.18	0.25	**0.61**	**0.01**	**0.12**	**0.22**
	MT	**0.41**	**0.01**	**0.30**	**0.48**	0.23	0.06	0.34	0.50	**0.40**	**0.01**	**0.30**	**0.47**
Chl_b	MAT	−0.02	0.45	0.12	0.18	−0.01	0.44	0.12	0.19	−0.01	0.43	0.12	0.18
	MNT	0.27	0.09	0.07	0.11	−0.14	0.84	0.09	0.11	0.26	0.09	0.07	0.11
	MT	0.08	0.18	0.20	0.29	0.06	0.20	0.20	0.28	0.08	0.18	0.20	0.28
Chl_{a+b}	MAT	0.30	0.00	0.20	0.31	0.15	0.03	0.22	0.33	0.31	0.00	0.20	0.28
	MNT	**0.53**	**0.02**	**0.08**	**0.15**	−0.02	0.39	0.12	0.16	**0.54**	**0.01**	**0.08**	**0.15**
	MT	0.24	0.05	0.28	0.44	0.16	0.10	0.30	0.43	0.24	0.05	0.28	0.42
$Chl_{a:b}$	MAT	**0.50**	**0.00**	**0.32**	**0.53**	0.15	0.03	0.41	0.61	**0.50**	**0.00**	**0.32**	**0.51**
	MNT	−0.02	0.38	0.28	0.41	0.33	0.06	0.23	0.37	0.01	0.34	0.28	0.39
	MT	0.12	0.13	0.32	0.36	0.04	0.25	0.33	0.41	0.12	0.13	0.32	0.39
Chl:Car	MAT	0.19	0.01	0.18	0.25	0.12	0.04	0.19	0.26	0.20	0.01	0.18	0.26
	MNT	0.01	0.34	0.21	0.30	−0.14	0.93	0.22	0.31	0.01	0.34	0.21	0.31
	MT	0.23	0.06	0.19	0.27	**0.53**	**0.00**	**0.15**	**0.21**	0.24	0.05	0.19	0.29

		nG^{-1} (CCI)				RG (PSRI)				RGr (ARI2)			
(b)		R^2	*P*-value	RMSE	RMSE-P	R^2	*P*-value	RMSE	RMSE-P	R^2	*P*-value	RMSE	RMSE-P
Chl_a	MAT	0.37	0.00	0.31	0.49	0.35	0.00	0.31	0.46	0.38	0.00	0.31	0.45
	MNT	**0.60**	**0.01**	**0.12**	**0.22**	**0.56**	**0.01**	**0.13**	**0.21**	**0.55**	**0.01**	**0.13**	**0.15**
	MT	0.39	0.01	0.31	0.47	0.35	0.02	0.32	0.47	0.36	0.02	0.31	0.47
Chl_b	MAT	−0.02	0.49	0.12	0.19	−0.02	0.44	0.12	0.19	0.00	0.36	0.12	0.19
	MNT	0.26	0.09	0.07	0.11	0.04	0.29	0.08	0.11	0.03	0.30	0.08	0.11
	MT	0.08	0.19	0.20	0.27	0.08	0.18	0.20	0.28	0.08	0.18	0.20	0.28
Chl_{a+b}	MAT	0.30	0.00	0.20	0.32	0.28	0.00	0.21	0.31	0.31	0.00	0.20	0.30
	MNT	**0.53**	**0.02**	**0.08**	**0.15**	**0.43**	**0.03**	**0.09**	**0.14**	**0.43**	**0.03**	**0.09**	**0.11**
	MT	0.24	0.05	0.28	0.41	0.23	0.06	0.28	0.42	0.23	0.06	0.28	0.41
$Chl_{a:b}$	MAT	**0.51**	**0.00**	**0.31**	**0.54**	**0.43**	**0.00**	**0.34**	**0.52**	**0.43**	**0.00**	**0.34**	**0.51**
	MNT	0.00	0.35	0.28	0.39	0.22	0.12	0.25	0.37	0.21	0.12	0.25	0.35
	MT	0.12	0.13	0.32	0.39	0.10	0.16	0.32	0.39	0.11	0.15	0.32	0.40
Chl:Car	MAT	0.19	0.01	0.18	0.27	0.20	0.01	0.18	0.26	0.23	0.01	0.18	0.24
	MNT	0.01	0.34	0.21	0.30	−0.05	0.46	0.21	0.31	−0.06	0.47	0.22	0.28
	MT	0.24	0.05	0.19	0.29	0.36	0.02	0.17	0.27	0.35	0.02	0.17	0.23

Notes: Veg, vegetation community; Pig, pigment content. Bold values represent moderate or stronger ($R^2 > 0.40$) significant linear regressions. MAT, moist acidic tussock tundra; MNT, moist non-acidic tundra; MT, moss tundra; RMSE, root mean square error. See Tables 1–3 for definitions of both spectral and RGB indices.

green sensors into an image pixel making green the most sensitive channel in the camera to mirror the sensitivity of the human eye (Bayer 1976).

From the standpoint of the human eye and digital cameras, all of the best performing RGB indices except one provide a measure of vegetation greenness and the weaker relationships seen with the carotenoid and anthocyanin (non-green pigments) indices are indicative of the cameras overall green bias or green sensitivity. The best performing RGB green band-based indices of 2G-RB, nG, nG^{-1}, RG, and rGR had the strongest relationships ($R^2 > 0.43$) with the pigment-driven spectral indices of PSSRb, PSSRa, CCI, PSRI, and ARI2, respectively, across all three vegetation communities. The moderate to strong relationships observed in all three communities suggest these RGB indices can be used to monitor seasonal vegetation changes associated with pigment-driven color changes, mostly related to the amount of green or chlorophyll pigments, in dominant low-Arctic vegetation communities

(Fig. 2). Though we found an overall weakness in RGB indices to accurately predict leaf-level pigment content, a number of significant weak to moderate relationships between Chl_a and Chl_{a+b} with the green RGB indices suggest they do capture seasonal changes in chlorophyll content. Moderate to weak relationships between pigment content and pigment-driven spectral indices have also been reported, even with data collected concurrently at the leaf level, due to variations in species-specific plant structure and developmental stage (Sims and Gamon 2002). The pigment content presented in this study is an approximation using the mean of dominant vascular species and does not take into account the influence of moss or standing litter, both of which influence greenness, especially at early and late season when vascular vegetation is not fully expanded. This combination of roughly estimated pigment content, a greenness signal that is not only composed of vascular species, especially at early and late season, and species-specific characteristics could explain the weak correlations and the differences between communities. However, it should be noted that all indices demonstrated a significant moderate correlation in at least one community with pigment content.

The five pigment-driven spectral indices used in this study target different pigment groups; however, all are relevant for the monitoring of foliar condition and photosynthetic activity suggesting the cameras can also indirectly infer changes to non-green pigment groups through an absence or changes in the greenness or chlorophyll pigments. Though the green RGB indices were generally the most consistent and had the strongest relationships, we also found that PRI is well represented by 2R-GB and nR in MT and MAT (Table 5; Appendix S1). Since the pigment-driven spectral index of PRI is a prominently used index for estimating photosynthetic light use efficiency (Gamon et al. 1992, Peñuelas et al. 1995, Gamon and Oecologia 1997), the use of digital camera nR to monitor this parameter is a particularly interesting result.

Current operational satellite missions provide an excellent opportunity for global monitoring of foliar condition with relatively high spatial resolution. Here we focused on exploring the spectral information in the visible wavelength region related to tundra vegetation color, driven by pigment dynamics. The broadband spectral settings of major operational satellite missions are at first consideration not optimal for capturing the detailed spectral reflectance of vegetation as represented by narrowband spectral vegetation indices. However, we show that RGB color values from consumer-grade digital cameras measuring even broader-band spectral information show correlations with reputed pigment-driven spectral indices such as CCI, PSSRa, and ARI2 indices. Our results suggest vegetation color contributes strongly to the response of these hyperspectral indices. The use of narrowband spectral indices related to vegetation color and pigment dynamics in order to monitor vegetation status and condition is already occurring with the Earth Observation System products from the Sentinel-2 multispectral satellite and will become more common in the future with upcoming hyperspectral satellite missions such as the Environmental Mapping and Analysis Program (EnMAP) planned for 2020.

Conclusions

Results of this study support the utility of digital cameras to act as a surrogate for in situ spectral data to monitor pigment dynamics as a result of seasonal changes in a low-Arctic ecosystem. The RGB indices using the green band perform best as proxies for pigment-driven spectral indices. We highlight nG as a proxy for PSSRa in particular because of moderate to strong relationships with both spectral and pigment data suggesting this RGB index can track changes in chlorophyll *a* content. We also suggest 2G-RB as a proxy for PSSRb, nG^{-1} for CCI, RG for PSRI, and RGr as a proxy for ARI1. Though the accuracy of pigment prediction for these indices is not as strong, there is evidence that RGB indices do track seasonal changes. This method represents a promising gap-filling tool and complimentary data source for optical remote sensing of vegetation in logistically and climatically challenging Arctic ecosystems. The implementation of low-cost time-lapse systems or nadir point measurements by an observer with consumer-grade digital cameras is highly feasible and proven in Arctic tundra ecosystems, and this study increases the possible applications of this method.

Acknowledgments

This research was supported by EnMAP science preparatory program funded under the DLR Space Administration with resources from the German Federal Ministry of Economic Affairs and Energy (support code: DLR/BMWi 50 EE 1348) in partnership with the Alfred Wegener Institute in Potsdam. Funding has also been provided through an NSERC Doctoral postgraduate scholarship awarded to AB. SC acknowledges support from the European Union's Horizon 2020 Research and Innovation Programme (Grant No: 689443) via the iCUPE project (Integrative and Comprehensive Understanding on Polar Environments). The authors would like to thank the logistical support provided by Toolik Research Station and Skip Walker of the Alaska Geobotany Center at the University of Alaska, Fairbanks. We would also like to thank Marcel Buchhorn and the HySpex Lab at the University of Alaska, Fairbanks for calibration of the spectrometer and MB and SW for providing GIS data of the Toolik Area. Finally, we would like to thank Robert Guy from the Faculty of Forestry at the University of British Columbia for laboratory support.

Literature Cited

Ahrends, H., S. Etzold, W. L. Kutsch, R. Stöckli, R. Brügger, F. Jeanneret, H. Wanner, N. Buchmann, and W. Eugster. 2009. Tree phenology and carbon dioxide fluxes: use of digital photography for process-based interpretation at the ecosystem scale. Climate Research 39:261–274.

Anderson, H. B., L. Nilsen, H. Tømmervik, S. Karlsen, S. Nagai, and E. J. Cooper. 2016. Using ordinary digital cameras in place of near-infrared sensors to derive vegetation indices for phenology studies of high Arctic vegetation. Remote Sensing 8:847.

Asner, G. P., and R. E. Martin. 2008. Spectral and chemical analysis of tropical forests: scaling from leaf to canopy levels. Remote Sensing of Environment 112:3958–3970.

Bartley, G., and P. Scolnik. 1995. Plant carotenoids: pigments for photoprotection, visual attraction, and human health. Plant Cell 7:1027–1038.

Bayer, B. 1976. Color imaging array. U.S. Patent 3,971,065.

Beamish, A., W. Nijland, M. Edwards, N. Coops, and G. Henry. 2016. Phenology and vegetation change measurements from true colour digital photography in high Arctic tundra. Arctic Science 2:33–49.

Bhatt, U., D. Walker, and M. Raynolds. 2010. Circumpolar Arctic tundra vegetation change is linked to sea ice decline. Earth Interactions 14:1–20.

Bhatt, U. S., D. A. Walker, M. K. Raynolds, P. A. Bieniek, H. E. Epstein, J. C. Comiso, J. E. Pinzon, C. J. Tucker, and I. V. Polyakov. 2013. Recent declines in warming and vegetation greening trends over pan-Arctic tundra. Remote Sensing 5:4229–4254.

Billings, W., and L. Bliss. 1959. An alpine snowbank environment and its effects on vegetation, plant development, and productivity. Ecology 40:388–397.

Bjorkman, A., S. Elmendorf, A. Beamish, M. Vellend, and G. Henry. 2015. Contrasting effects of warming and increased snowfall on Arctic tundra plant phenology over the past two decades. Global Change Biology 21:4651–4661.

Blackburn, G. 1998. Spectral indices for estimating photosynthetic pigment concentrations: a test using senescent tree leaves. International Journal of Remote Sensing 19:657–675.

Blackburn, G. 1999. Relationships between spectral reflectance and pigment concentrations in stacks of deciduous broadleaves. Remote Sensing of Environment 70:224–237.

Blackburn, G. A. 2007. Wavelet decomposition of hyperspectral data: a novel approach to quantifying pigment concentrations in vegetation. International Journal of Remote Sensing 28:2831–2855.

Bratsch, S. N., H. E. Epstein, M. Buchhorn, and D. A. Walker. 2016. Differentiating among four Arctic tundra plant communities at Ivotuk, Alaska using field spectroscopy. Remote Sensing 8:51.

Chalker-Scott, L. 1999. Environmental significance of anthocyanins in plant stress responses. Photochemistry and Photobiology 70:1–9.

Close, D., and C. Beadle. 2003. The ecophysiology of foliar anthocyanin. Botanical Review 69:149–161.

Cook, B., and E. Wolkovich. 2012. Divergent responses to spring and winter warming drive community level flowering trends. Proceedings of the National Academy of Sciences 109:9000–9005.

Coops, N., T. Hilker, C. Bater, M. Wulder, S. Nielsen, G. McDermid, and G. Stenhouse. 2012. Linking ground-based to satellite-derived phenological metrics in support of habitat assessment. Remote Sensing Letters 3:191–200.

Coops, N., T. Hilker, F. Hall, C. Nichol, and G. Drolet. 2010. Estimation of light-use efficiency of terrestrial ecosystems from space: a status report. BioScience 63:788–797.

Coops, N., C. Stone, D. Culvenor, L. Chisholm, and R. Merton. 2003. Chlorophyll content in eucalypt vegetation at the leaf and canopy scales as derived from high resolution spectral data. Tree Physiology 23:23–31.

Curran, P. J. 1989. Remote sensing of foliar chemistry. Remote Sensing of Environment 30:271–278.

Demmig-Adams, B., and W. W. Adams. 1996. The role of xanthophyll cycle carotenoids in the protection of photosynthesis. Trends in Plant Science 1:21–26.

Elmendorf, S. C., et al. 2012*a*. Plot-scale evidence of tundra vegetation change and links to recent summer warming. Nature Climate Change 2:453–457.

Elmendorf, S., et al. 2012*b*. Global assessment of experimental climate warming on tundra vegetation: heterogeneity over space and time. Ecology Letters 15:164–175.

Esteban, R., et al. 2009. Alternative methods for sampling and preservation of photosynthetic pigments and tocopherols in plant material from remote locations. Photosynthesis Research 101:77–88.

Féret, J.-B., C. François, A. Gitelson, G. Asner, K. Barry, C. Panigada, A. Richardson, and S. Jacquemoud. 2011. Optimizing spectral indices and chemometric analysis of leaf chemical properties using radiative transfer modeling. Remote Sensing of Environment 115:2742–2750.

Gamon, J., F. Huemmrich, C. Wong, I. Ensminger, S. Garrity, D. Hollinger, A. Noormets, and J. Peñuelas. 2016. A remotely sensed pigment index reveals photosynthetic phenology in evergreen conifers. Proceedings of the National Academy of Sciences 113:13087–13092.

Gamon, S., and S. Oecologia. 1997. The photochemical reflectance index: an optical indicator of photosynthetic radiation use efficiency across species, functional types, and nutrient levels. Oecologia 112: 492–501.

Gamon, J., J. Peñuelas, and C. Field. 1992. A narrow-waveband spectral index that tracks diurnal changes in photosynthetic efficiency. Remote Sensing of Environment 41:35–44.

Garbulsky, M., J. Peñuelas, J. Gamon, Y. Inoue, and I. Filella. 2011. The photochemical reflectance index (PRI) and the remote sensing of leaf, canopy and ecosystem radiation use efficiencies a review and meta-analysis. Remote Sensing of Environment 115:281–297.

Gitelson, A. A., G. P. Keydan, and M. N. Merzlyak. 2006. Three-band model for noninvasive estimation of chlorophyll, carotenoids, and anthocyanin contents in higher plant leaves. Geophysical Research Letters 33:LL1402.

Gitelson, A., and M. Merzlyak. 1998. Remote sensing of chlorophyll concentration in higher plant leaves. Advances in Space Research 22:689–692.

Gitelson, A. A., M. N. Merzlyak, and O. B. Chivkunova. 2001. Optical properties and nondestructive estimation of anthocyanin content in plant leaves. Photochemistry and Photobiology 74:38–45.

Gitelson, A. A., M. N. Merzlyak, and H. K. Lichtenthaler. 1996. Detection of red edge position and chlorophyll content by reflectance measurements near 700 nm. Journal of Plant Physiology 148:501–508.

Gitelson, A. A., Y. Zur, O. B. Chivkunova, and M. N. Merzlyak. 2002. Assessing carotenoid content in plant leaves with reflectance spectroscopy. Photochemistry and Photobiology 75:272–281.

Gould, K. S., J. McKelvie, and K. R. Markham. 2002. Do anthocyanins function as antioxidants in leaves? Imaging of H2O2 in red and green leaves after mechanical injury. Plant, Cell and Environment 25:1261–1269.

Høye, T. T., E. Post, N. M. Schmidt, K. Trøjelsgaard, and M. C. Forchhammer. 2013. Shorter flowering seasons and declining abundance of flower visitors in a warmer Arctic. Nature Climate Change 3:759–763.

Ide, R., and H. Oguma. 2010. Use of digital cameras for phenological observations. Ecological Informatics 5:339–347.

Ide, R., and H. Oguma. 2013. A cost-effective monitoring method using digital time-lapse cameras for detecting temporal and spatial variations of snowmelt and vegetation phenology in alpine ecosystems. Ecological Informatics 16:23–34.

Iler, A. M., T. T. Høye, D. W. Inouye, and N. M. Schmidt. 2013. Nonlinear flowering responses to climate: Are species approaching their limits of phenological change? Philosophical Transactions of the Royal Society B 368:20120489.

Inouye, D. W., and D. A. McGuire. 1991. Effects of snowpack on timing and abundance of flowering in *Delphinium nelsonii* (Ranunculaceae): implications for climate change. American Journal of Botany 78:997–1001.

Merzlyak, M., A. Gitelson, O. Chivkunova, and V. Rakitin. 1999. Non-destructive optical detection of pigment changes during leaf senescence and fruit ripening. Physiologia Plantarum 106:135–141.

Migliavacca, M., M. Galvagno, E. Cremonese, M. Rossini, M. Meroni, O. Sonnentag, S. Cogliati, G. Manca, F. Diotri, and L. Busetto. 2011. Using digital repeat photography and eddy covariance data to model grassland phenology and photosynthetic CO_2 uptake. Agricultural and Forest Meteorology 151:1325–1337.

Mutanga, A. Skidmore., and H. H. Prins. 2004. Predicting in situ pasture quality in the Kruger National Park, South Africa, using continuum-removed absorption features. Remote Sensing of Environment 89:393–408.

Mutanga, O., and A. Skidmore. 2004. Hyperspectral band depth analysis for a better estimation of grass biomass (*Cenchrus ciliaris*) measured under controlled laboratory conditions. International Journal

of Applied Earth Observation and Geoinformation 5:87–96.

Nijland, W., D. R. Jong, D. Jong, and M. Wulder. 2014. Monitoring plant condition and phenology using infrared sensitive consumer grade digital cameras. Agricultural and Forest Meteorology 184:98–106.

Park, T., S. Ganguly, H. Tømmervik, E. S. Euskirchen, K.-A. Høgda, S. Karlsen, V. Brovkin, R. R. Nemani, and R. B. Myneni. 2016. Changes in growing season duration and productivity of northern vegetation inferred from long-term remote sensing data. Environmental Research Letters 11:084001.

Parmentier, F.-J., and T. Christensen. 2013. Arctic: speed of methane release. Nature 500:529.

Peñuelas, J., I. Filella, and J. A. Gamon. 1995. Assessment of photosynthetic radiation-use efficiency with spectral reflectance. New Phytologist 131:291–296.

Porra, R. J., W. A. Thompson, and P. E. Kriedemann. 1989. Determination of accurate extinction coefficients and simultaneous equations for assaying chlorophylls a and b extracted with four different solvents: verification of the concentration of chlorophyll standards by atomic absorption spectroscopy. Biochimica et Biophysica Acta (BBA): Bioenergetics 975:384–394.

Prevéy, J., et al. 2017. Greater temperature sensitivity of plant phenology at colder sites: implications for convergence across northern latitudes. Global Change Biology 23:2660–2671.

R Development Core Team. 2007. R: a language and environment for statistical computing. R Foundation for Statistical Computing, Vienna, Austria.

Richardson, A., J. Jenkins, B. Braswell, D. Hollinger, S. Ollinger, and M.-L. Smith. 2007. Use of digital webcam images to track spring green-up in a deciduous broadleaf forest. Oecologia 152:323–334.

Sims, D. A., and J. A. Gamon. 2002. Relationships between leaf pigment content and spectral reflectance across a wide range of species, leaf structures and developmental stages. Remote Sensing of Environment 81:337–354.

Steyn, W. J., S. J. E. Wand, D. M. Holcroft, and G. Jacobs. 2002. Anthocyanins in vegetative tissues: a proposed unified function in photoprotection. New Phytologist 155:349–361.

Stylinski, C., J. Gamon, and W. Oechel. 2002. Seasonal patterns of reflectance indices, carotenoid pigments and photosynthesis of evergreen chaparral species. Oecologia 131:366–374.

Tieszen, L. L. 1972. The seasonal course of aboveground production and chlorophyll distribution in a wet arctic tundra at Barrow, Alaska. Arctic and Alpine Research 4:307–324.

Ustin, S. L., and B. Curtiss. 1990. Spectral characteristics of ozone-treated conifers. Environmental and Experimental Botany 30:293–308.

Ustin, S., A. Gitelson, and S. Jacquemoud. 2009. Retrieval of foliar information about plant pigment systems from high resolution spectroscopy. Remote Sensing of Environment 113:S67–S77.

Walker, M. D., D. A. Walker, K. R. Everett, and C. Segelquist. 1989. Wetland soils and vegetation, arctic foothills, Alaska. U.S. Fish and Wildlife Service Biological Report 89, Washington, D.C., USA.

Walker, M., et al. 2006. Plant community responses to experimental warming across the tundra biome. Proceedings of the National Academy of Sciences USA 103:1342–1346.

Westergaard-Nielsen, A., M. Lund, B. Hansen, and M. Tamstorf. 2013. Camera derived vegetation greenness index as proxy for gross primary production in a low Arctic wetland area. ISPRS Journal of Photogrammetry and Remote Sensing 86:89–99.

Wheeler, H., T. Høye, N. Schmidt, J.-C. Svenning, and M. Forchhammer. 2015. Phenological mismatch with abiotic conditions—implications for flowering in Arctic plants. Ecology 96:775–787.

Young, A., and G. Britton. 1990. Carotenoids and stress. Pages 87–112. *in* R. G. Alscher and J. R. Cummings, editors. Stress Responses in Plants: Adaptation and Acclimation Mechanisms. Wiley-Liss, New York, New York, USA.

Yu, H., E. Luedeling, and J. Xu. 2010. Winter and spring warming result in delayed spring phenology on the Tibetan Plateau. Proceedings of the National Academy of Sciences 107:22151–22156.

Zhang, X., D. Tarpley, and J. T. Sullivan. 2007. Diverse responses of vegetation phenology to a warming climate. Geophysical Research Letters 34:L19405.

Supporting Information

Additional Supporting Information may be found online at: http://onlinelibrary.wiley.com/doi/10.1002/ecs2.2123/full